Energy Reports 8 (2022) 7789–7799

Contents lists available at ScienceDirect

Energy Reports

journal homepage: www.elsevier.com/locate/egyr

Research paper

Implementation of a solar aided refrigration unit for refrigerated trucks employing photovoltaic generators

Antonio Rossetti [a,*], Sergio Marinetti [a], Paolo Artuso [b], Francesco Fabris [c], Silvia Minetto [a]

[a] National Research Council, Construction Technologies Institute, Corso Stati Uniti 4, 35127 Padova, Italy
[b] Bsim ITALY, Corso Generale Giuseppe Govone, 18, 10129 Torino, Italy
[c] Università degli Studi di Padova, via Venezia 1, Padova, 35127, Italy

ARTICLE INFO

Article history:
Received 31 March 2022
Received in revised form 27 May 2022
Accepted 31 May 2022
Available online xxxx

Keywords:
Refrigerated transport
Photovoltaic systems
Solar-aided refrigeration
Refrigerated road vehicle

ABSTRACT

Solar aided refrigeration system can represent a simple and feasible solution for improving the sustainability of refrigerated transport. The paper presents the design and the performance of an electric powered refrigeration unit integrated with photovoltaic generators installed on top of the refrigerated box of a light truck. The system prototype has been tested in stationary conditions, demonstrating the capacity of the solar system to impact significantly in the net energy balance of the refrigeration unit. The system performance during an urban multi-drop delivery scenario and hot climatic condition are then assessed using a dynamic lumped model simulation. Simulations are also used to discuss the sensitivity to the battery pack capacity size and the shading conditions caused by the urban canyon effects are investigated. Results demonstrate that, on a yearly base at Athens climatic conditions, the solar panels can provide from 65% to 112% of the energy consumed by the cooling unit, depending on the time spent by the truck under direct sunlight. Larger batteries are justified only when long periods of direct light are expected.

1. Introduction

Refrigerated transport is one of the most critical links in the cold chain, being in charge of guaranteeing goods safety and quality at many stages of the products life, under challenging boundary conditions, thus contributing to reduce food losses and the overall carbon footprint food chain. In addition, when considering local transport and last mile delivery, the refrigerated vehicle needs to be evaluated in terms of local pollution and air quality, as the refrigeration unit contributes to the overall vehicle emissions. On the other side, this sector is quite resistant to innovation. The possible improvements listed by Cavalier, 2011 are still relevant to this sector: the enhancement of the insulation capabilities, the optimization of the external aerodynamics of the boxes, and the optimization of the refrigeration units and their control.

While in long-haul refrigerated trailers a dedicated diesel engine powers up the refrigerated unit, in short-distance refrigerated vehicles the traction diesel engine runs also the refrigerated unit's compressor. Both options have a relevant impact on the environment. Lawton et al. (2019) documented that NOx and particulates emissions caused by nose-mounted refrigeration units can be one order of magnitude greater than the one imposed to a Euro VI engine. On the other side, Fabris et al. (2020) studied the increase in emissions in a direct-driven refrigeration unit for a small truck: the emission of CO and THC due to the vehicle traction increase by 25% as the result of the refrigeration unit. Tassou et al. (2009) reported different figures to describe the environmental impact of refrigerated road transport concluding that the engine driven food transport refrigeration systems can contribute to 40% of the emissions of the vehicle engine.

In addition to the emission increase, the direct connection of the refrigeration unit to the traction engine is particularly critical also in terms of performances. The cooling power is, in fact, unrelated to the actual cooling demand as the compressor speed varies proportionally to the engine speed. This possibly leads the unit to deliver the lower cooling capacity when high cooling power is requested. For example, the time required to recover the temperature set point after a door opening cycle can be increased if the vehicle is idle, and as demonstrated by Estrada-Flores and Eddy (2006), this time is a significant key performance indicator of the goods temperature variability.

The uncoupling between the diesel engine and the compressor can be achieved by using an electric generator connected to engine powering an electric hermetic compressor (Cavalier and Tassou, 2011). This layout enables the implementation of control logics aimed at minimizing the overall fuel

* Corresponding author.
E-mail address: antonio.rossetti@itc.cnr.it (A. Rossetti).

https://doi.org/10.1016/j.egyr.2022.05.284

Nomenclature

Subscrips and Superscripts

se	external surface
i	internal
ON	referred to the ON period of the cooling unit
Battery	referred to the battery pack
Ref. Unit	refrigeration unit
PV	photovoltaic panels
Net	net energy flow to the battery
ev	evaporator
conv	convective
rad	radiative
sun	solar
amb	ambient
inf	infiltration
comp	compressor
is	isoentropic
mec	mechanical
IN	compressor inlet
OUT	compressor outlet
r	refrigerant
a	transported goods

Symbols

a_s	*surface adsorptivity* (–)
A	area (m^{-2})
C	thermal capacity (J kg^{-1} K^{-1})
e	state of charge (–)
E	energy (J)
G_{dh}	diffuse solar radiation (W m^{-2})
G_f	direct solar radiation (W m^{-2})
h	enthalpy (J kg^{-1})
$\overline{k}$	*vertical unit vector* (–)
K	Overall heat transfer coefficient (W m^{-2} K^{-1})
$\dot{m}$	refrigerant mass flowrate (kg s^{-1})
$\overline{n}$	*normal unit vector* (–)
p	pressure (Pa)
P	electrical power (W)
$\dot{Q}$	heat transfer (W)
S	Box external surface (m^2)
T	Temperature (K)
t	time (s)
v	vehicle speed (m s^{-1})
V	volume (m^{-1})
α_{fc}	forced convection coefficient (W m^{-2} K^{-1})
α_{nc}	natural convection coefficient (W m^{-2} K^{-1})
ϵ	surface emissivity (–)
η	*efficiency* (–)
ρ	density (kg m^{-3})

consumption by desynchronizing the electric power production at the internal combustion engine and the power consumption at the compressor and is a prerequisite to develop more complex and efficient systems based on natural refrigerants as the CO_2 refrigeration unit with multiple configurations presented by Fabris et al. (2021a,b). Furthermore, the electrification of the refrigeration unit compressor opens to the integration of renewables in the system, limiting the reliance of the cooling unit on fossil fuels.

Literature regarding the use of photovoltaic driven or aided refrigeration unit in the transport sector is limited and often dated.

Bahaj (1998, 2000) reported the results achieved testing a full-electrified system, obtained by replacing the diesel generator of conventional trailers with a battery pack. Photovoltaic panels installed on the trailer roof contributed to the energy balance, recharging the battery pack when solar radiation was available. According to the Author's conclusions, the absence of a backup power unit to supply energy once the batteries are fully discharged was a major critical point: in order to avoid cold chain interruption, the user has to check the battery status and to plan the system recharging in advance.

In the same years, the Sandia National Laboratories conducted an extensive feasibility study for chilled and refrigerated long distance transport (Bergeron, 2001). The study proved the technological feasibility of these systems but only a moderate economic justification.

Following the results presented by Bahaj in 1998 and 2000, Elliston and Dennis (2009) carried out a second study on the feasibility of PV-assisted electrified refrigerated transport of frozen goods. The thermal load was evaluated by a simple 0D thermodynamic model, in which the thermal load applied to the inner contents is the sum of the conductive heat load through the walls for average daily temperature data (by month) in Canberra (Australia) and the refrigerator thermal power. The sizing of the components was supported by the estimation of the PV production. The feasibility study concluded that the proposed system was economically unattractive as results of the low pricing of the diesel fuel in Australia at that time.

In the last years, the improvements in the solar panel and battery technology had led to a revision of the conclusion proposed in these early studies coupling photovoltaic generators and refrigeration systems for both stationary and mobile applications. Meneghetti et al. (2018), for example, discussed the impact of the optimal design of a rooftop solar photovoltaic system coupled with an automated cold storage. The same Authors (Meneghetti et al., 2021a,b) discussed the application of solar generators to semitrailers for chilled and frozen goods, sizing the system capacity to match the energy request of the refrigeration systems considering both daily and seasonal changes for different climatic conditions.

Other studies focus on the application of the solar generators as a sustainable solution to support the cold chain in developing countries. For example, Kumar and Bharj (2018, 2019) reported the study of a three wheeled plug-in light vehicle with solar panel designed for the delivery of perishable goods. The solution was discussed in terms of potential benefits and challenges for the reduction of food losses and the lowering of carbon emissions in urban areas during last mile delivery. Buitendach et al. (2019) presented the use of solar powered Peltier refrigerated storage to preserve vaccines at controlled temperature during transportation in remote regions. The system could maintain the design temperature for 72 h with 1 °C accuracy.

These examples available in the literature mainly discuss the actual economical and technical sustainability of the proposed solutions, and they do not seem to completely cover the different vehicle and applications involved in the cold chain. Furthermore, when numerical simulation are employed to discuss these systems, dynamics are usually neglected adopting quasi stationary approach and a simplistic description of the components efficiencies and characteristics.

Table 1
Main external dimensions of the insulated box.

Height [m]	2.00
Length [m]	3.00
Width [m]	2.00
Surface [m^2]	32.0

This paper presents the feasibility study and the preliminary experimental test of a vapour compression cycle aided by electrical energy provided by photovoltaic panels. Conversely to the available literature, that considered plug-in long-distance transport (Bahaj, Bergeron, Elliston and Dennis and Meneghetti) or small scale distribution (Kumar) with limited transport capacity, this study focuses on a short-distance refrigerated delivery truck. To reduce the battery capacity and to guarantee the cooling capacity, a hybrid solution is adopted. The system runs normally on a battery pack that can be pre-charged from the electrical grid and is recharged by the solar panels when the solar radiation is available. Nevertheless, to extend the system autonomy, the system can also rely on the vehicle internal combustion engine to guarantee functionality and food safety.

The first part of the paper presents the case study identified and the experimental results of a preliminary stationary test, run to characterize the main components and to verify the robustness of the system design. Then a dynamic numerical model of the truck cooling system, refrigerated box, electrical and control system is presented and run to assess the impact of the renewable energy on the energy consumption of the truck assuming a daily delivery mission in an urban area. The model accounts for the infiltration associated to the doors opening at each delivery and the convective and radiative thermal exchange between the refrigerated box and the ambient. The sensitivity of the system performance on the battery size and the shading due to the urban canyon effects are discussed. Results are presented both on a daily and a seasonal scale.

2. Case study

2.1. The reference system

For the present study, the insulated body of a small, refrigerated truck, available in the market, is considered as test case. Its external dimensions are reported in Table 1. The overall internal volume is 9.75 m^3, with a double door covering the whole rear face and a smaller side door.

The box is made of a polyurethane foam coated both on the internal and external sides with 1.5 mm fiberglass layer. Due to the small size of the considered box, no wooden reinforcements are included in the roof or the sidewalls, while a plywood plate and an array of wood beams reinforce the floor.

For the sake of simplicity, the box, where 0 °C internal conditions are required, is equipped with a vapour compression refrigeration unit working with R134a, representative of the standard technology for this application, although environmentally friendly solutions based on Natural Working Fluids (NWF) are currently under development or already out in the field as for the case of CO2 (Fabris et al., 2021a,b) and Propane (Kivevele, 2022). The compressor is driven by a DC electrical motor and runs at constant speed thus the cooling capacity is modulated by means of an on–off controller with 3 °C of hysteresis. Fig. 1 reports the main components of the refrigeration unit, as well as its integration with the photovoltaic panels.

The reference system was preliminary tested at the ATP test station of the Construction Technology Institute of the National Research Council in Padua (Italy), to assess the overall heat transfer coefficient (K) according the internal heating method prescribed by the ATP standard (Fig. 2a). The measured K value was 0.36 W m^{-2} K^{-1}. The average COP and cooling capacity for a set point internal temperature of −2 °C and an external temperature of 30 °C were assessed. The cooling demand was estimated based on the global heat transfer coefficient previously obtained:

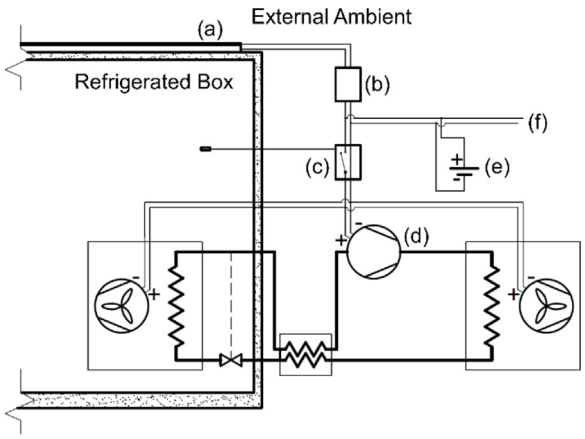

Fig. 1. Refrigeration system integrated with photovoltaic generators: (a) photovoltaic panels; (b) charge regulator; (c) on–off thermostat; (d) compressor; (e) battery pack; (f) backup line connected to the vehicle alternator.

$$\overline{Q} = KS(T_{ext} - \overline{T_{int}}) \tag{1}$$

$$\overline{Q_{ON}} = \frac{\overline{Q}}{DC} \tag{2}$$

$$COP_{ON} = \frac{\overline{Q_{ON}}}{P_{Ref.Unit}} \tag{3}$$

resulting on an average cooling power during the ON time $\overline{Q_{ON}} = 1.02$ kW and a $COP_{ON} = 0.86$.

2.2. Integration of the photovoltaic generator in the existing system

The reference system is modified in order to include the photovoltaic generators, connected by means of a charge regulator to a battery pack which power the refrigeration unit.

The photovoltaic generators (a, Fig. 1) are sized to cover the roof of the insulated box. Due to the limited area available (6 m^2), six panels are installed, leading to a nominal power of 940 W for 5.4 m^2 of active surface. A charge-controller (b) is used in order to optimize the panel conversion efficiency and to transform the panel voltage to 24 V recharging the battery pack (e). The charge controller is also responsible for reducing the generated power when the battery pack reaches the maximum charge. Four high capacity Pb–Ca car batteries are used, obtaining a nominal overall capacity $E_{battery} = 8640$ kJ with 24 V nominal tension.

The refrigeration unit compressor (d) and fans are powered by the 24 V battery pack. In order to guarantee the cooling power required to maintain the refrigerated box at the design temperature, a backup power line (f) is included in the system. This line is powered by the vehicle alternator and can sustain the cooling unit in case the battery pack is fully discharged.

The backup line can be used also to recharge the battery pack and run the system from the electrical grid when the vehicle is not is use or during the pulldown before the loading.

Fig. 2. Experimental Set-up: (a) insulated box characterization in the ATP test facility; (b) Stationary experimental set-up.

3. Stationary experimental tests

Experimental activities were conducted in order to verify the overall layout and demonstrate the capabilities of the solar generators to contribute significantly to the cooling unit energy demand under steady condition. The experimental set up is presented in Fig. 2b: the insulted box is positioned in full sun position, with the solar panel fixed to an OBS panel over the roof of the insulated box. While the solar panels are designed to fit the roof area of the box, a larger surface is needed in this set up, as some clearance is provided between the photovoltaic generators in order to allow an inspection path. The prototype is equipped with temperature and humidity sensors to monitor both the internal and the external temperature. The power flows are monitored by recording the battery voltage and the electric currents by means of Hall effect current transducers.

The experimental facility was located in the north of Italy (N°45.39 E°11.93) and was placed so to be unaffected by the shadows of the surrounding buildings. Data were recorded in June 2019, including a non-stop run of a week between the 23rd of June and the 1st of July. Data acquisition was carried out using an Arduino Mega board logging the data with a period of two seconds. Two different data set are presented in this manuscript. In the first (24th June) the pull-down is performed: the cooling unit is switched on after two days of inactivity at 8:30 in the morning and then maintained active. This will be referred as Scenario A. In the second data set (29th June), the unit is running continuously since the first start of the system 5 days before. This will be referred as Scenario B.

Fig. 3a reports the power produced by the solar generators from 6:00 to 21:00 and the solar radiation for the first data set. The power produced by the solar panel is initially close to zero, as the charge controller limits the power production in order to avoid overcharging the battery pack in absence of the load. Once the cooling unit is switched on at 8:30, the charge regulator allows producing the maximum power, to recharge the energy used during the pulldown (Fig. 3b). The produced power follows then the same trend of the solar radiation until 12:00. At this point, the energy produced by the solar panel is sufficient to fully recharge the battery pack. The charge regulator thus limits the power production at the end of every on–off cycle, leading to progressive reduction of the produced power as highlighted in Fig. 3b.

Since the refrigeration units works on an on–off cycle while the energy produced by the solar panel is continuous, the instant power consumption reported in Fig. 3b and 3c is not suitable to compare the overall energy balance of the system over the whole day. The data are then post processed to obtain a visualization of the average power for every on–off cycle, obtaining the histogram in Fig. 4. Fig. 5 instead presents the cumulative energy demand considering the overall consumed energy and the net energy trend, normalized on the nominal battery capacity, assuming the batteries are fully charged before the start of the day:

$$e_{Ref.Unit} = 1 - \frac{\int_{00:00}^{t} P_{Ref.Unit}\, d\tau}{E_{battery}} \tag{4}$$

$$e_{Net} = 1 - \frac{\int_{00:00}^{t} P_{Ref.Unit} - P_{PV}\, d\tau}{E_{battery}} \tag{5}$$

As expected, the first cycle containing the pull-down has a high average power and the photovoltaic panel can compensate only a small fraction of the energy requested by the cooling unit (Fig. 4), corresponding to a sudden decrease of the energy stored in the battery pack (Fig. 5). On the contrary, in the middle hours of the day, when the solar panel can produce more energy than the average energy consumed by the refrigeration unit, there is an increase in the battery charge level that becomes stable at around 84% of the nominal value. This equilibrium is then maintained until the late afternoon (18:00): at this point, the solar radiation quickly decreases, while the cooling unit maintains a high cooling demand due to the high external temperature. Furthermore, a scheduled electrical defrost is performed at 18:00 (represented by the peak in the refrigeration unit power request in Fig. 4), that speeds up the battery discharge.

Figs. 6–8 report the data of the second data set, in which the refrigerated box is already at the design temperature, so that no pull down is required. This scenario can be representative of a truck not fully unloaded between two consecutive working days, where the cooling unit is powered using the engine or the grid energy during the night. Despite the panels can contribute only during daytime, it is evident that in this case they can provide a great part of the daily energy requested by the cooling unit.

In order to quantify the impact of the renewable energy in the system, the energy produced by the solar panel can be normalized on the overall consumption of the cooling unit:

$$\beta(t) = \frac{E_{Net} - E_{Ref.Unit}}{1 - E_{Ref.Unit}} = \frac{\int_{00:00}^{t} P_{PV}\, d\tau}{\int_{00:00}^{t} P_{Ref.Unit}\, d\tau} \tag{6}$$

This ratio is clearly dependent on the time and decreases as the evaluation time is moved to the late afternoon. Table 2 reports

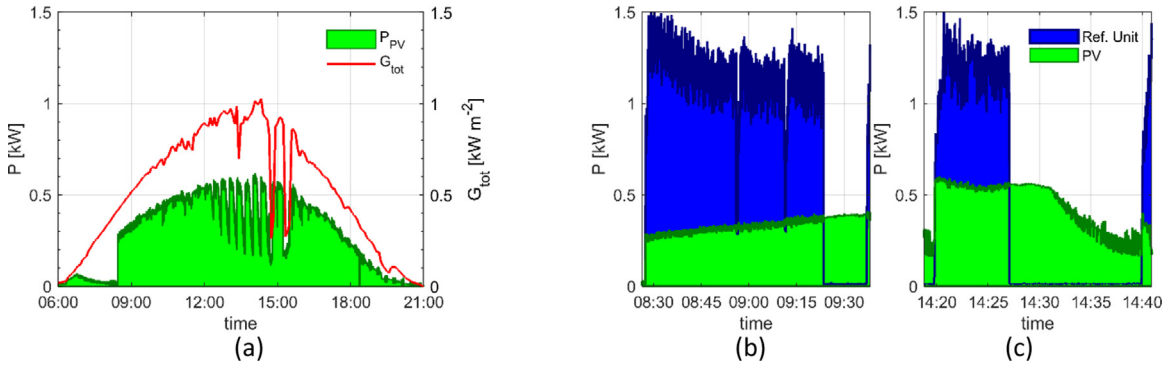

Fig. 3. Solar power production—Scenario A: (a) daily power production trend and solar radiation; (b) and (c) highlight of the refrigeration unit power consumption and solar power production during an on–off cycle.

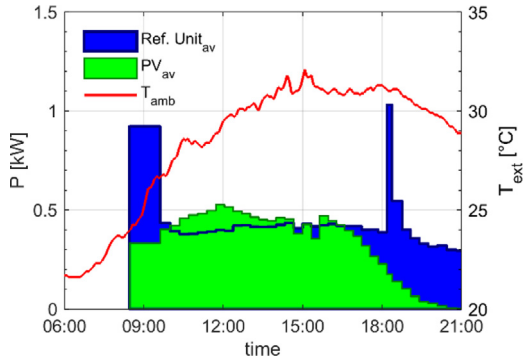

Fig. 4. Refrigeration unit power consumption and photovoltaic panels generated power averaged over on–off cycle—Scenario A.

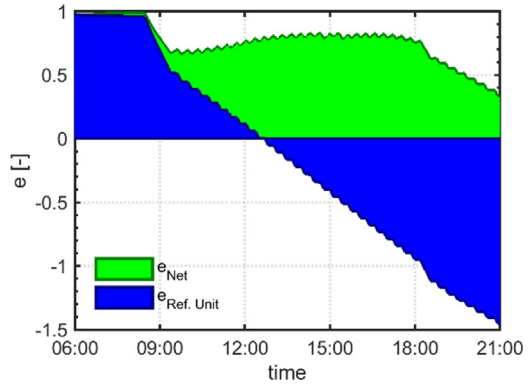

Fig. 5. Cumulative net energy consumption and refrigeration unit energy consumption—Scenario A.

Table 2
Ratio of renewable energy over the refrigeration unit overall consumption.

	Reference ending time		
	13:00	18:00	24:00
Scenario A - pull down at 9:00	83.7%	88.6%	65.5%
Scenario B - stabilized temperature	53.7%	70.0%	56.0%

this ratio considering as ending time 13:00, 18:00 and 24:00 representative of a half-day, full working day and continuous use of the unit for the two data set previously presented.

Experimental results reported in Table 2 demonstrate the actual capacity of the presented system of significantly reducing the request for external energy of the refrigeration unit. The limited extent of the experimental campaign and the stationary nature of the experimental apparatus prevent any generalization of the reported data to the system actual working conditions. In order to guess the impact on a mobile application, a numerical model is developed and used to simulate the system under a daily delivery mission under different ambient condition.

4. Numerical simulations

As the preliminary test demonstrated an interesting potential of the solar system in supporting the cooling unit, numerical simulations are conducted to forecast the system performance during a delivery service, thus considering the effects of door opening and the vehicle velocity. The dynamic 0D commercial software Simecenter Amesim v17 is used for simulations.

4.1. General equations and boundary conditions

The model solves the temperatures and the energy fluxes of a refrigerated truck during an urban delivery mission. It is made of three main model-blocks: the refrigerated box, the cooling unit and the solar system (see Fig. 9).

The internal air is accounted for as a capacitive model characterized by the internal air thermal capacity and its average temperature T_i, which is solved by means of an energy balance equation:

$$\frac{C_i dT_i}{dt} = \dot{Q}_{convi} + \dot{Q}_{inf} - \dot{Q}_{ev} \tag{7}$$

where $\dot{Q}_{convi}$ is the heat flow exchanged between the air and the internal walls by convection; $\dot{Q}_{inf}$ accounts for the energy transported by the air infiltrating the box when the doors are open while $\dot{Q}_{ev}$ is the heat flow removed by the cooling unit. The external air infiltration is estimated according to the model reported by Lafaye De Micheaux et al. (2015), that solves the air exchange based on the geometrical data of the box and of its opening and the temperature difference between the inside and the external ambient.

The internal wall temperature is obtained by solving the dynamic response of the refrigerated box model.

The conduction through the insulated body is solved by discretizing the refrigerated box thickness in 10 elements with proper thermal resistance and capacity. These values are optimized to approximate the experimental dynamic response of the box as discussed in detail in Artuso et al. (2019).

The external surface temperature is then obtained by setting the equilibrium between the conduction heat flow through the

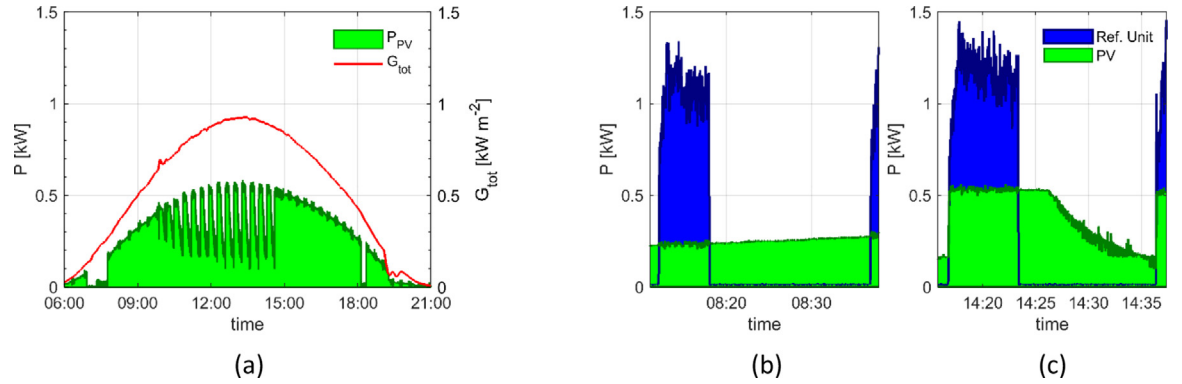

Fig. 6. Solar power production—Scenario B: (a) daily power production trend and solar radiation; (b) and (c) highlight of the refrigeration unit power consumption and solar power production during on–off cycle.

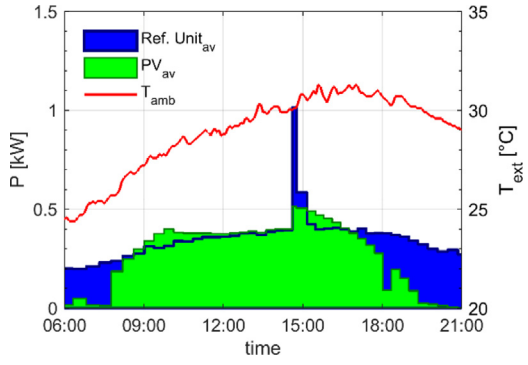

Fig. 7. Refrigeration unit power consumption and photovoltaic panels generated power averaged over on–off cycle—Scenario B.

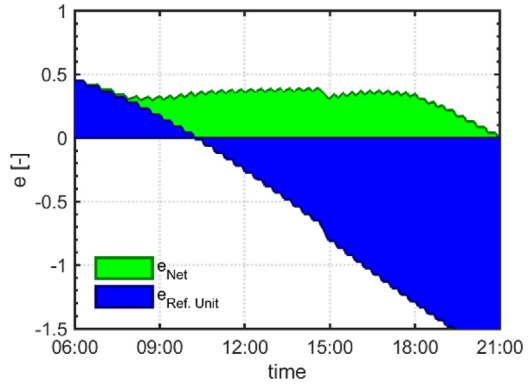

Fig. 8. Cumulative net energy consumption and refrigeration unit energy consumption—Scenario B.

insulated wall and the external loads, accounting for the contribution of the solar radiation and the convective and radiative exchange with the ambient:

$$\dot{Q}_e = \dot{Q}_{conve} + \dot{Q}_{sun} + \dot{Q}_{rade} \tag{8}$$

External convection is assumed as the maximum heat flow between natural convection and forced convection, expressed as a function of the vehicle speed v:

$$\dot{Q}_{conve} = \max\left(\alpha_{nc}, \alpha_{fc}(v)\right)\left(T_{amb} - T_{se}\right) Se \tag{9}$$

Natural and forced convective coefficients are modelled using standard flat plate correlation (ASHRAE, 2009).

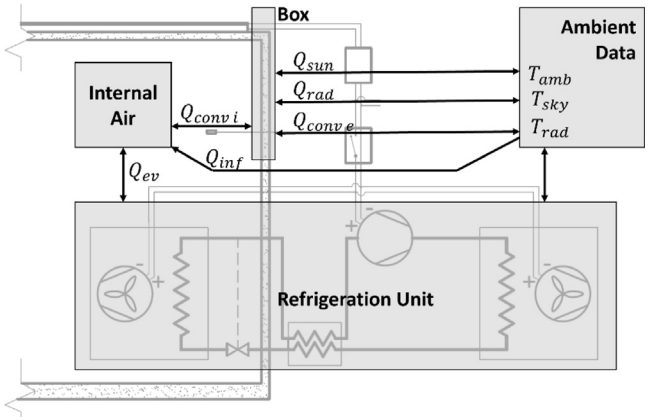

Fig. 9. Schematic representation of the main elements and heat fluxes considered in the numerical model.

The solar radiation applies to the box external surfaces, accounting for direct and diffuse radiation. As the amount of direct radiation intercepted by the vertical surfaces of the box is a function of the angle between the truck travelling direction and the sun, an average condition is computed as the integral mean between all the possible truck orientations:

$$\dot{Q}_{sun} = \frac{\int_{\theta=0}^{\theta=\pi} a_s \left(G_{dh} - \overline{n(\theta)} \cdot \overline{G_f}\right) dS_e}{\pi} \tag{10}$$

where θ is the angle between the truck front and the North direction.

The radiative heat transfer between the environment and the sky is instead evaluated as:

$$\dot{Q}_{rade} = \sigma \varepsilon \left(\frac{1 + \overline{n} \cdot \overline{k}}{2} \left(T_{sky}^4 - T_{se}^4\right) + \frac{1 - \overline{n} \cdot \overline{k}}{2} \left(T_{rad}^4 - T_{se}^4\right) \right) \tag{11}$$

The fictive sky temperature is calculated by assuming the sky to be an ideal black surface and can be determined according to (DOE United States Department of Energy, 2015), while the reference ambient temperature for the radiative exchange with the surroundings T_{rad} is assumed as the equilibrium temperature of a vertical white surface subject to the solar radiation and natural convection.

The fiberglass composite white surface of the truck is characterized using surface absorptivity a_s is set to 0.15, and surface emissivity ϵ to 0.70 according to Rossi et al. (2013). These values are then locally modified in Eqs. (10) and (11) if the photovoltaic panels are included. Further details are given in Section 4.4.

Table 3
Boundary condition.

	Variables
Ambient data	T_{amb}, T_{sky}
Solar radiation	G_{dh}, G_f
Vehicle	v

The boundary conditions of the numerical model are reported in Table 3.

4.2. The truck model

The refrigerated body characteristics reflect those the box used in the stationary mock-up presented in the previous session.

The insulated body is modelled as a series of thermal capacities and resistance tuned to fit the steady (global heat transfer coefficient) and dynamic response of the refrigerated body. The details of this procedure are presented and discussed in Artuso et al. (2019).

4.3. The refrigeration unit

According to the unit used in the experimental activities, a simple vapour compression cycle using R-134a is considered for the model with a cooling power of 3.3 kW, at the reference condition of $T_i = 0$ °C and $T_{amb} = 30$ °C. The compressor model is developed using as reference a 400 cm ^{3} compressor specifically realized for transport application. The performance maps in terms of efficiencies as a function of the inlet conditions and the pressure ratio were interpolated on the base of the manufacturer catalogue (Bitzer, 2021)

The volumetric efficiency η_{vol} and the overall compression efficiency η_{comp} has been computed given the tabular compressor data. The overall compression efficiency η_{comp} is then conventionally divided into the mechanical efficiency η_{mec} (including ventilation losses and electrical conversion) and the isentropic efficiency η_{is} which include the heat dispersed by the compressor body. Given the efficiencies, the working conditions and the thermodynamic status of the refrigerant at the compressor inlet, the discharge conditions, the mass flow rate and the power drawn can be computed as follow:

$$\dot{m}_r = \rho_{IN} \frac{\omega}{60} V_d \eta_{vol} \tag{12}$$

$$P_{comp} = \frac{\dot{m}_r \Delta h_{is}}{\eta_{comp}} = \frac{\dot{m}_r \Delta h_{is}}{\eta_{mec}\eta_{is}} \tag{13}$$

$$h_{OUT} = h_{IN} + \frac{P_{comp}}{\dot{m}_r} \tag{14}$$

Evaporator and condenser are characterized by 8.9 m^2 and 7.5 m^2 external heat transfer surface. The fin and tube heat exchangers are modelled as ideal counter-flow tube in tube configuration heat exchangers, discretizing the flow in six lumped volumes of equal area. Each of this exchange elements is composed by three elementary components. The first describes the convective exchange on the refrigerant side. The second describes the conduction through the metal accounting for thermal conduction and capacity. The third element models the convective exchange on the air side.

Eqs. (15) and (16) express the mass continuity and energy balance on the refrigerant side for each element:

$$V_r^{(j)} \left(\frac{\partial \overline{\rho}_r}{\partial p}\bigg|_h^{(j)} \frac{d\overline{p}_r^{(j)}}{dt} + \frac{\partial \overline{\rho}_r}{\partial h}\bigg|_p^{(j)} \frac{d\overline{h}_r^{(j)}}{dt} \right) = \dot{m}_r^{(j)} - \dot{m}_r^{(j-1)} \tag{15}$$

$$V_r^{(j)} \left[\left(\overline{h}_r^{(j)} \frac{\partial \overline{\rho}_r}{\partial p}\bigg|_h^{(j)} - 1 \right) \frac{d\overline{p}_r^{(j)}}{dt} + \left(\overline{h}_r^{(j)} \frac{\partial \overline{\rho}_r}{\partial h}\bigg|_p^{(j)} + \overline{\rho}_r^{(j)} \right) \frac{d\overline{h}_r^{(j)}}{dt} \right] = \dot{m}_r^{(j-1)} \overline{h}_r^{(j-1)} - \dot{m}_r^{(j)} \overline{h}_r^{(j)} - \dot{Q}_{convr}^{(j)} \tag{16}$$

The convective term in Eq. (16) represents the convective exchange between the fluid and the tube wall. More details on the numerical simulation set-up of the units can be found in Artuso et al. (2020) and Fabris et al. (2020).

A 10 K superheating is imposed by means of PI controlled lamination valve, while the unit is controlled by a simple on–off thermostat set to switch on the unit when the temperature reaches the 2 °C and to switch off the unit once the internal temperature reaches the −1 °C.

4.4. The solar system

The Solar generators are located on top of the insulated box, in contact with the roof. This assumption has the effect of increasing slightly the cooling need of the refrigerated box by increasing both the surface emissivity and the short-wave absorptivity with respect to the white fiberglass composite (from 0.7 and 0.15 to 0.8 and 0.9 respectively). Nevertheless, this installation is preferred as the presence of an air gap between the solar panels and the box roof can potentially lead to greater problems such as vibration, noise and structural problems caused by the aerodynamic interaction when the vehicle is in motion.

The panels' efficiency at standard conditions η_{pv} is evaluated from the manufacturer data sheet and is equal to 0.21. The electrical converted power is computed as:

$$P_{pv} = \eta_{pv} A \left[G_{dh} - \overline{n} \cdot \overline{G_f} \right] \tag{17}$$

where A is the total area of the panels.

As the fraction of the solar energy converted in electrical power is not degraded to thermal energy, the term P_{pv} must be subtracted from Eq. (8) partially compensating for the increase of $\dot{Q}_{sun}$ and $\dot{Q}_{rade}$ as results of the local increase in the absorptivity and emissivity caused by the photovoltaic panels.

4.5. Mission profile and ambient data

The mission profile describes an urban distribution activity. The truck is supposed to start its mission outside the urban area, in a logistic facility. At 6.00 AM the refrigeration unit is switched on to pull down the refrigerated box temperature, then at 8.00 AM the truck is loaded. It drives to the urban area and starts a series of driving – delivery cycles after which it drives back to the logistic facility.

To define the vehicle time–velocity table, the World harmonized Light-duty vehicles Test Procedure (WLTP) cycle is used to build the daily mission of the truck. The driving time between the logistic facility and the urban area is modelled using two Rural (high velocity) and two Suburban (medium velocity) cycles, corresponding to approximatively 24 km in 30 min. The driving - delivery cycle is simulated using two Urban (low velocity) cycles followed by a 5-minute stop to allow the delivery to be performed, for an overall of 6 km in 25 min (including the 5 min stop). This cycle is repeated 7 times before driving outside the urban area. The whole driving cycle is repeated two times in a day, starting at 9.00 AM and at 2.00 PM.

The refrigeration unit is supposed to start one hour before the vehicle departure (8.00 AM), to cool down the refrigerated box mass to the transportation temperature.

The ambient external conditions are derived by the standard climatic year data (Anon EnergyPlus, 2021) of Athens to represent

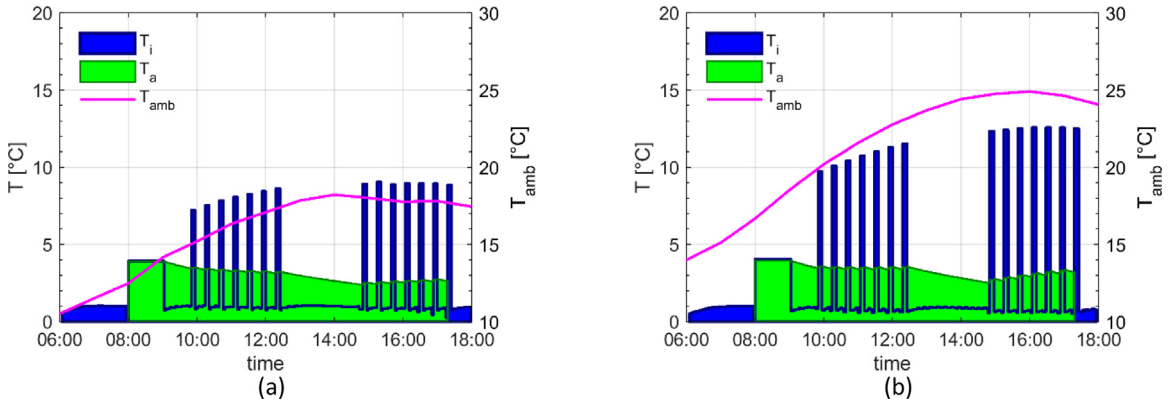

Fig. 10. Internal, external and transported goods temperatures averaged over each on–off cycle: (a) May; (b) August.

the European climatic condition. In particular, the ambient temperature and humidity, and the solar radiation data are used as boundaries for the model. For each month, the ambient variables are averaged to obtain a reference day representative for the entire month instead of using a particular day in the month. This latter option is abandoned during the preliminary tests as the sky cover and the solar radiation can have important discontinuities between consecutive days, leading to results that are excessively dependent on the day chosen as a reference.

To prevent an arbitrary initialization to affect the simulation results, simulation is run for several full days (in simulation time) under cyclic boundary conditions, until all the model state variables reached a periodic response, verified by comparing the system status at the mission beginning at 6:00 AM between two consecutive cycles.

The initialization is then carried out independently for each set of boundary condition/system presented in the results section.

5. Numerical results

Simulations are run for the average day of each month of the year in order to collect data on the impact of the changes in both the solar radiation available and the average ambient temperature during the year. Results are presented in two sections. The first result session shows and details the outcomes for May and August, in order to discuss in detail, the system performance in the mid-season and in the hot season. Then, in the following section, the integral results of the other months are discussed to assess the impact of the photovoltaic panel on the energy performance of the refrigeration unit on a yearly base.

5.1. Mission result in warm (May) and hot climate (August)

August is the reference month to discuss the results, being the most severe month in the year for the refrigerating system due to its high average temperature; results obtained in August are compared to those in May, to highlight how the different ambient temperature and solar radiation affect the unit performance. Fig. 10 reports the internal temperature averaged over each on–off duty cycle, the temperature of the transported goods and the ambient temperature. Results demonstrate the capability of the chosen refrigeration unit to maintain an almost constant internal temperature T_i and to guarantee a fast recovery of the desired temperature after each door opening.

In fact, the temperature of the transported goods T_a is always below 4 °C despite the frequent doors opening.

The refrigeration unit power input is reported in Fig. 11 in comparison with the power delivered by the solar panels. The refrigeration unit average power presents many peaks that exceed the solar power production. These can be associated to three different events. The first corresponds to the pull down of the insulated box at the beginning of the mission. The second, which is shorter than the first, happens when the unit is switched on after the loading, when the cooling unit works to remove the heat stored in the walls during the loading operations. The third event causing a significant increase in the unit power consumption is the door opening, associated with the delivery that is repeated seven times in the morning and seven times in afternoon. As this increase in power consumption is due to the external air entering the box, it is not surprising that the absolute value of peaks after each opening follows the same trend of the ambient temperature (Fig. 10).

According to the scheme in Fig. 1, the unit is supposed to run on the batteries, as long as the batteries are able to provide the requested energy. When the batteries are totally discharged and the instant power requested by the refrigeration unit is greater than the power provided by the photovoltaic panels, the refrigerating unit relies on an external power source, i.e. the vehicle alternator. On the other side, the battery can store the power produced by the photovoltaic panels that exceeds the instant consumption of the refrigerated unit. The system performances are then sensitive to the battery nominal capacity: larger batteries increase the system autonomy, reduce the need for external power source but increase the system mass and cost.

To discuss the effect of the battery pack capacity, three nominal capacities are compared in this work corresponding to 2.16, 4.32 and 8.64 MJ, initializing the battery at the mission start to half of their nominal charge. Fig. 12 reports the nominal stored energy for different capacities of the battery pack for the two reference months. The negative ordinate axis represents the cumulative energy taken from the external energy source.

The photovoltaic panels produce more energy than consumed by the refrigeration unit during long travel periods and the long stop between the two delivery missions, leading to an increase of the stored energy both in May and August. On the other side, the pull down and the distribution activity results are strongly affected by the external ambient conditions. For the most part of the delivery activity, a negative net energy balance is achieved, leading to a progressive discharge of the battery. Nevertheless, as a remarkable exception, when the May mission is considered, thanks to the mild ambient temperature, the system can produce more energy than the one used to reset the internal temperature after each door opening, leading to a progressive recharge of the battery pack. The effects of the finite capacity of the battery on the daily energy balance can be seen comparing the starting and the ending charge for each capacity. In mild climatic condition (Fig. 12a) the larger the battery pack, the higher the energy

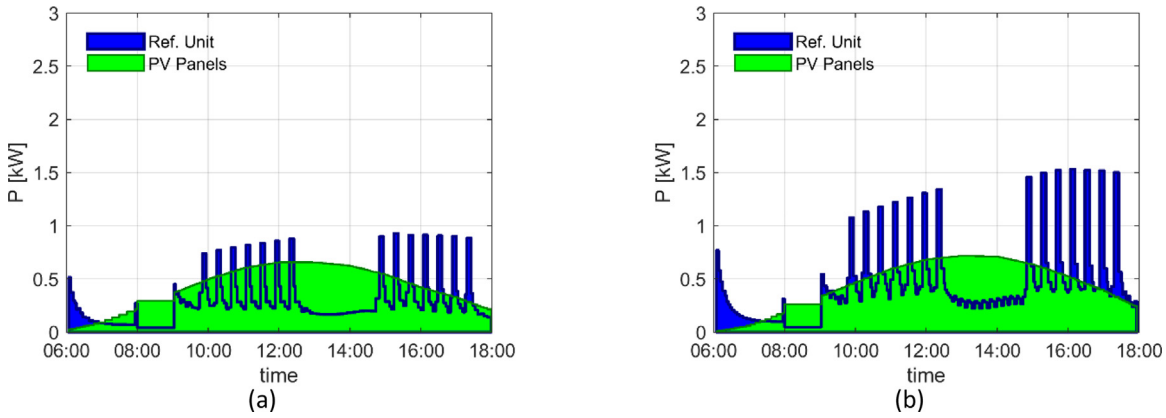

Fig. 11. Refrigeration unit power consumption and photovoltaic panels generated power averaged over each on–off cycle: (a) May; (b) August.

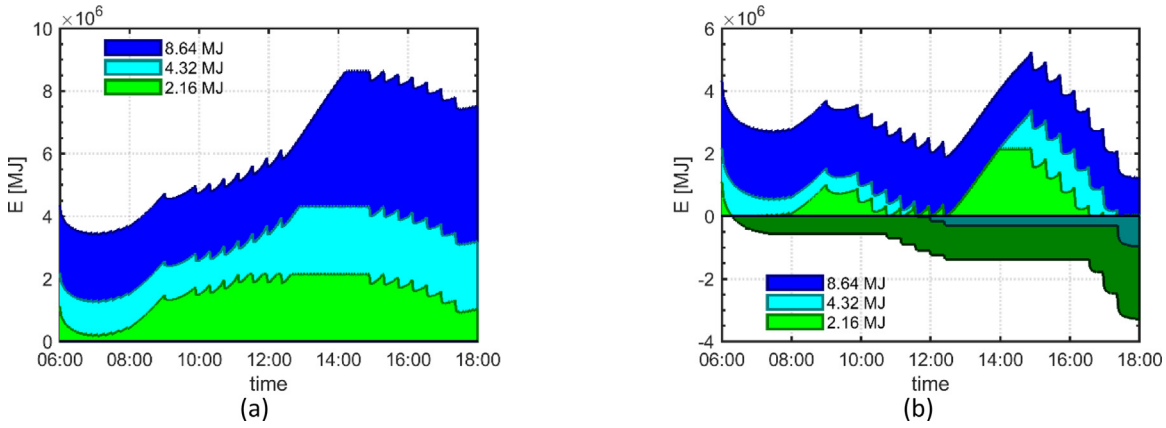

Fig. 12. Nominal battery charge status: (a) May; (b) August. [Negative values in 12b represents the energy drawn from the external source].

balance as more energy can be store during the central hours of the day before the full charge condition actives the charge regulator limiter. Under this climatic condition and the model assumptions, all the capacities can run the system without resorting to the backup power supply. When the hot climatic condition is considered (Fig. 12b), each battery pack presents a different behaviour. The two higher capacity batteries present almost the same behaviour once the graph is shifted accordingly to the different initial value. For both the cases, the capacities reach the same overall daily balance of −1.25 MJ. However, while the larger one (8.64 MJ) does not draw power from the backup source, the 4.32 MJ capacity one is fully discharged twice, requiring the system to run on the external source at the end of each delivery session. On the other side, when the smallest battery pack is considered, the overall energy balance is −2.75 MJ as the charge regulator limits the panels' power production when the battery is fully charged at 2 PM, thus wasting some available energy due to the limited battery capacity.

5.2. Yearly results

The same mission described in Section 4.5 is run under the average ambient data of every month.

The daily ideal energy production that is computed as the integral of all the power produced by the photovoltaic panels during the day is reported in Fig. 13a. It exceeds the energy used by the refrigeration unit for the largest part of the year: August is the only month with a substantial difference between production and demand, while September and October are slightly negative. As previously discussed, the finite capacity of the battery pack must be considered in order to obtain a better estimation as it can strongly affect the daily energy imbalance. Fig. 13b reports the net energy balance of the battery pack assuming the smaller and larger capacity presented in Fig. 12: respectively 2.16 MJ and 8.64 MJ. These data are compared to the case where no panels are installed, and the refrigeration unit runs draining energy from the vehicle alternator. The presence of the solar system reduces significantly the energy drained from the vehicle for both the larger and the smaller battery capacity. The main difference between the two arrangements is visible during the first half of the year, where the largest capacity leads to a significant net energy gain, which can contribute to sustain the vehicle auxiliary systems such as lightning and air conditioning systems.

5.3. Sensitivity to the urban canyon effect

The ambient data used for the simulation already account for the effect of sky cover, like fog or clouds, as the direct solar radiation is obtained as the average for the considered month. On the other side, the delivery takes mostly place in an urban environment, where the urban canyon structure can affect the amount of solar radiation collected by the photovoltaic panel, reducing it to the distributed solar radiation when the truck is covered by the shadow of a nearby building.

The actual amount of direct radiation collected by the solar panel can be obtained only assuming the structure of the urban environment: urban canyon aspect ratio, average length and orientation. This might reduce the usefulness of the results as different configurations can lead to contrasting results.

In order to discuss the impact of the urban environment three abstract cases are considered here. The first is the one already

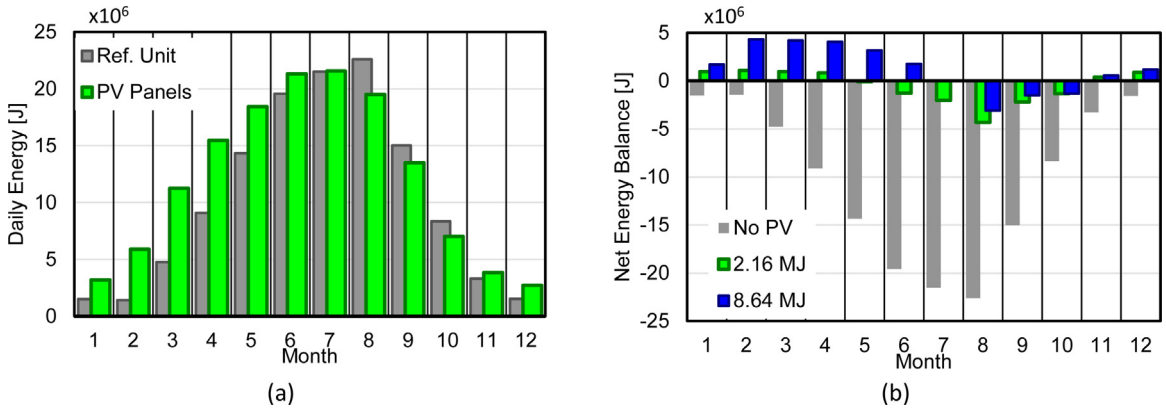

Fig. 13. Yearly Results: (a) Daily energy produced by the photovoltaic panels and consumed by the refrigeration unit; (b) Net daily energy balance for different nominal battery capacity.

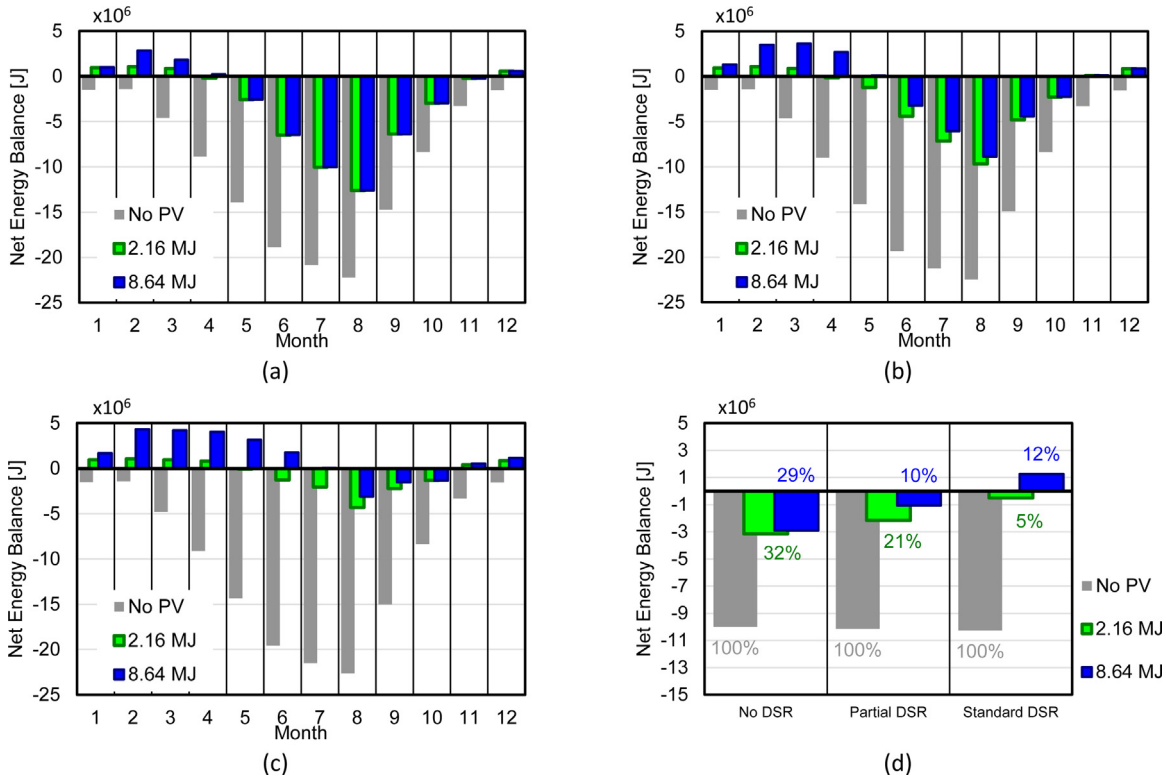

Fig. 14. Net energy balance as function of the shading condition in the case of no solar system (No PV), and for a nominal battery capacity of 2.16 and 8.64 MJ: (a) No DSR, i.e., worst-case scenario; (b) Partial-DSR; (c) Full-DSR, i.e. best-case scenario; (d) yearly average net energy balance (percentage expressed using the No PV as reference).

presented in Section 5.2, where the Global Horizontal Radiation (GHR) is taken directly from the ambient data. This represents the best-case scenario, and it will be referred as Full-GHR. In the worst-case scenario, the Direct Solar Radiation (DSR) is neglected for the whole time of the mission, assuming that only the Diffuse Horizontal Radiation (DHR) contributes to the GHR. This case will be referred as No-DSR. The last case represents an intermediate condition, assuming the DSR to be obscured only when the truck is driving in the urban environment (Partial-DSR).

The results are presented in Fig. 14.

Figs. 14a–c suggest that the larger battery pack can be exploited efficiently only when the shading is limited and the system can collect the direct solar radiation: in fact, when the diffuse radiation is considered the differences between the results of the two battery capacities are negligible. Fig. 14d summarizes the average yearly results. The presence of the solar panels can play an important role also when the direct solar radiation is neglected, reducing the power drain from the vehicle to one third with respect to the case without the photovoltaic panels. The system becomes more and more efficient as more direct solar radiation is considered, lowering the energy request to the 5% (2.16 MJ battery pack) or producing a net energy excess of the 12% (8.64 MJ battery pack) when the ambient data are considered without modification. Fig. 14d allows also quantifying the advantage of a larger battery pack. While for shaded condition (No DSR) the performances between the two batteries capacity are similar ($\Delta E \cong 3\%$), the larger pack allows to efficiently take advantage of the direct radiation. When the Partial DSR is considered, the

difference rises to $\Delta E \cong 11\%$ that becomes $\Delta E \cong 17\%$ when the Standard DSR is considered.

6. Conclusions

The paper presents an electric powered refrigeration system integrated with photovoltaic generators built on the top of the refrigerated box. The solar system aims at reducing the energy drawn by the refrigeration unit from the vehicle prime engine and at using the battery pack to sustain the peak requests and to store electric energy produced for a later use. A stationary test of the system is presented as well as numerical dynamic model to assess the impact of the photovoltaic panels on the system in an urban delivery mission. The experimental data demonstrate the capacity of the solar system to contribute to the overall energy balance under early summer condition in northern Italy climate, providing the 94% of the energy required to run the system between 6.00 and 18.00.

Numerical simulations on a dynamic lumped model software are then run to assess the performance of this system during an urban delivery mission with frequent stops and door openings in a hot climate (Athens). The sensitivity to battery pack capacity size and the shading conditions caused by the urban canyon effects is investigated. The results demonstrated that the solar panel could provide, as an average through the year, more than 65% of the energy required by the cooling unit on a daily mission in the worst-case scenario, i.e. when the environment shades the truck and no direct light hit the panels. If the shading due to obstacle is partial, the photovoltaic panels can reduce by 95% power drawn from the vehicle alternator. Larger battery packs are justified when the truck is expected to run with moderate or limited shading from buildings or other sources. In this case, a larger battery pack can improve the performance up to 17%, leading to a net +12% energy excess on yearly base.

The results thus justify further research towards these hybrid solutions to reduce noise and emissions in urban areas. Further development of this research on the experimental side will focus on the design of a fully functional prototype to demonstrate the actual performance of such architectures. On the numerical side, the contribution of solar energy to the overall vehicle energy balance should be discussed for different truck type and missions profile. Another topic to be investigated is the net contribution to the reduction of GWP emissions once the system is assessed in terms of life cycle assessment. Finally, the replacement of the R134a refrigeration unit, merely used as a reference, with a NWF system, is to be evaluated in combination with the presented solution as a way towards zero or drastic reduction of GWP emissions related to the refrigeration system of transport vehicles.

CRediT authorship contribution statement

Antonio Rossetti: Conceptualization, Methodology, Software, Writing – original draft, Funding acquisition. **Sergio Marinetti:** Supervision, Project administration. **Paolo Artuso:** Software, Validation. **Francesco Fabris:** Software, Writing – original draft, Writing – review & editing. **Silvia Minetto:** Methodology, Writing – review & editing, Funding acquisition.

Declaration of competing interest

The authors declare the following financial interests/personal relationships which may be considered as potential competing interests: Antonio Rossetti reports financial support was provided by ISOKIT S.r.L.

Acknowledgements

The research activity presented in this paper was carried out in collaboration with ISOKIT S.r.L. In particular, the Authors acknowledge the support and the contribution to this research given by Mr. Andrea Antico and Mr. Dario Zennaro.

References

Anon EnergyPlus, 2021. https://energyplus.net/ (last visited 22 April 2021).
Artuso, P., Marinetti, S., Minetto, S., Col, D., Del, Rossetti, A., 2020. Modelling the performance of a new cooling unit for refrigerated transport using carbon dioxide as the refrigerant. Int. J. Refrig. 115, 158–171.
Artuso, P., Rossetti, A., Minetto, S., Marinetti, S., Moro, L., Del Col, D., 2019. Dynamic modeling and thermal performance analysis of a refrigerated truck body during operation. Int. J. Refrig. 99, 288–299.
ASHRAE, 2009. ASHRAE fundamentals handbook (SI). Chapter4.
Bahaj, A.S., 1998. World's first solar powered transport refrigeration system. Renew. Energy 15 (1–4), 572–576.
Bahaj, A.S., 2000. Photovoltaic power for refrigeration of transported perishable goods. In: Conference Record of the Twenty-Eighth IEEE Photovoltaic Specialists Conference. 15-22 Sept. 2000, Anchorage, AK, USA.
Bergeron, D., 2001. Solar powered refrigeration for transport application – a feasibility study. Sandia Rep. Sand 200, 1–3753.
Bitzer, 2021. Catalogue data. www.bitzer.de (last accessed 22 April 2021).
Buitendach, H., Jiya, I.N., Gouws, R., 2019. Solar powered peltier cooling storage for vaccines in rural areas. Indones J. Electr. Eng. Comput. Sci..
Cavalier, G., Tassou, S., 2011. Sustainable refrigerated road transport. In: 21st Informatory Note on Refrigerating Technologies. International Institute for Refrigeration.
DOE United States Department of Energy, 2015. EnergyPlus engineering reference version 8.2: The reference to EnergyPlus calculations. In: The Reference to EnergyPlus Calculations. pp. 92–94.
Elliston, B., Dennis, M., 2009. Feasibility of solar-assisted refrigerated transport in Australia. In: The 47th ANZSES Annual Conference. 29 Sept.–2 Oct. Townsville, Queensland, Australia, In: Solar09.
Estrada-Flores, S., Eddy, A., 2006. Thermal performance indicators for refrigerated road vehicles. Int. J. Refrig. 29, 889–898.
Fabris, F., Artuso, P., Marinetti, S., Minetto, S., Rossetti, A., 2021a. Dynamic modelling of a CO2 transport refrigeration unit with multiple configurations. Appl. Therm. Eng. 1895, 116749.
Fabris, F., Artuso, P., Marinetti, S., Minetto, S., Rossetti, A., 2021b. Dynamic modelling of a CO2 transport refrigeration unit with multiple configurations. Int. J. Refrig. 189.
Fabris, F., Artuso, P., Rossetti, A., Minetto, S., Marinetti, S., 2020. Impact of the refrigeration system on the fuel consumption and on the emissions of a small refrigerated truck. In: 6th IIR International Conference on Sustainability and the Cold Chain. August 26-28, Nantes, France.
Kivevele, T., 2022. Propane (HC – 290) as an alternative refrigerant in the food transport refrigeration sector in southern Africa – a review. Autom. Exp. 5 (1), 75–89, 2022.
Kumar, S., Bharj, R.S., 2018. Energy consumption of solar hybrid 48v operated mini mobile cold storage. In: IOP Conf Ser Mater Sci Eng. p. 455.
Lafaye De Micheaux, T., Ducoulombier, M., Moureh, J., Sartre, V., Bonjour, J., 2015. Experimental and numerical investigation of the infiltration heat load during the opening of a refrigerated truck body. Int. J. Refrig. 54, 170–189.
Lawton, R., Mynott, T., Marchall, N., Wagner, F., 2019. Emission testing of transport refrigeration unit. In: 25th IRR International Congress of Refrigeration. Montreal, Canada.
Meneghetti, A., Dal Magro, F., Romagnoli, A., 2021a. Renewable energy penetration in food delivery: Coupling photovoltaics with transport refrigerated units. Energy 232, 1–11.
Meneghetti, A., Dal Magro, F., Romagnoli, A., 2021b. Renewable energy penetration in food delivery: Coupling photovoltaics with transport refrigerated units. Energy 232, 1–11.
Meneghetti, A., Dal Magro, F., Simeoni, P., 2018. Fostering renewables into the cold chain: How photovoltaics affect design and performance of refrigerated automated warehouses. Energies 11 (5), 1029.
Rossi, S., Bison, P., Bortolin, A., Cadelano, G., Ferrarini, G., Libbra, A., Muscio, A., 2013. In field evaluation of the absorption coefficient of the external surface of the insulated box in a refrigerated vehicle. In: Proceedings of the 2nd IIR International Conference on Sustainability and the Cold Chain. Paris, April 2-4.
Tassou, S.A., De-Lille, G., Ge, Y.T., 2009. Food transport refrigeration – approaches to reduce energy consumption and environmental impact of road transport. Appl. Therm. Eng. 29, 1467–1477.